

## Supporting Information

### **d-Band Center Modulation and Surface Pt-O Bonding Promoted Pt Nanoparticles with High Performance for Stable pH-Universal Hydrogen Evolution at Ampere-Level Current Densities**

*Xin Wang,<sup>‡a</sup> Yongjie Wang,<sup>‡b</sup> Zhongqing Jiang,<sup>c</sup> Binglu Deng<sup>d</sup> and Zhong-Jie Jiang<sup>\*a</sup>*

<sup>a</sup> Guangzhou Key Laboratory for Surface Chemistry of Energy Materials, Guangdong Engineering and Technology Research Center for Surface Chemistry of Energy Materials, New Energy Research Institute, College of Environment and Energy, South China University of Technology, Guangzhou 510006, China. E-mail: eszjiang@scut.edu.cn

<sup>b</sup> Guangdong Provincial Key Laboratory of Semiconductor Optoelectronic Materials and Intelligent Photonic Systems, Harbin Institute of Technology, Shenzhen 518055, China.

<sup>c</sup> Zhejiang Key Laboratory of Quantum State Control and Optical Field Manipulation, Department of Physics, Zhejiang Sci-Tech University, Hangzhou 310018, China.

<sup>d</sup> School of Materials Science and Hydrogen Energy, Foshan University, Foshan 528000, China.

<sup>‡</sup> These authors contribute equally to this work.

## **1. Experimental section**

### **1.1 Chemicals and materials**

All the chemicals were directly utilized as received with further purification. Carbon nanotubes (CNTs with <3% amorphous carbon) of 40-60 nm in diameter and 5-15  $\mu\text{m}$  in length were purchased from Shenzhen Nanotech Port Co. Ltd. Chloroplatinic acid hydrate ( $\text{H}_2\text{PtCl}_6 \cdot 6\text{H}_2\text{O}$ , Pt $\geq$ 37.5%), urea (99%), and aniline (95%) were obtained from Shanghai Macklin Biochemical Ltd. Ammonium peroxodisulfate (APS, 98%) and ethanol absolute (99.7%) were bought from Tianjin Damao Chemical Reagent Co. Ltd. Nitric acid ( $\text{HNO}_3$ ,  $\geq$ 68%) and sulfuric acid ( $\text{H}_2\text{SO}_4$ , 98%) were bought from Guangzhou Chemical Reagents Co. Pt/C (20 wt.%) was bought from Shanghai Aladdin Bio-Chem Technology Co. Ltd. Nafion (5.0 wt.% in isopropanol) was obtained from Dupont China Holding Ltd. Deionized water with resistance of  $18.2 \text{ M}\Omega \text{ cm}^{-1}$  was used for all the experiments.

### **1.2 Synthesis of Pt/CNTs**

2.0 g of the CNTs were functionalized through refluxing in a mixed solution with 120.0 mL of  $\text{H}_2\text{SO}_4$  and 40.0 mL of  $\text{HNO}_3$  at 80  $^\circ\text{C}$  for 4 h. The surface functionalized CNTs with a good hydrophilicity were then washed thoroughly by centrifugation until the pH values of the supernatant were close to 7.0 and finally dispersed in water to give a concentration of 5.0 mg  $\text{mL}^{-1}$ .

For the growth of Pt NPs, 3.0 mL of the prepared CNTs solution was dispersed in 15.0 mL of anhydrous ethanol. 15.0 mL of water was added to make the volume ratio of ethanol:water = 1.0:1.0. After good dispersion by ultrasonication (> 10 min), 200.0 mg of urea was added, followed by the injection of 1.0 mL of a  $\text{H}_2\text{PtCl}_6$  solution (0.03 mmol  $\text{mL}^{-1}$ ). The reaction solution was then transferred to a 50.0 mL autoclave and hydrothermally reacted at 140  $^\circ\text{C}$  for 2 h. After cooling, the Pt/CNTs was collected by centrifugation and washing several times with anhydrous ethanol and dried at 60  $^\circ\text{C}$  for the subsequent uses.

### 1.3 Synthesis of C@Pt/CNTs

20.0 mg of the Pt/CNTs synthesized above were mixed with 20.0 mL of water under ultrasonication. The reaction mixture was then placed in an ice-water bath. 5.0 mL of HCl (0.5 M) solution containing 60.0 mg APS and 5.0 mL of HCl (0.5 M) solution containing 30.0  $\mu$ L aniline were sequentially injected. The reaction was lasted for  $\sim$ 10 h. The obtained PANI@Pt/CNTs were collected through centrifugation and washing > 3 times with ethanol and calcined in a tube furnace at 325 °C. The obtained product was named as C@Pt/CNTs-325.

For comparison, the samples of PANI@Pt/CNTs-200, C@Pt/CNTs-300, Pt/CNTs-400, and Pt-500 were also prepared by the calcination of the PANI@Pt/CNTs at 200, 300, 400, and 500 °C, respectively. The Pt/CNTs-325 was prepared by the direct calcination of the Pt/CNTs at 325 °C in air. The C@Pt/CNTs-325(N<sub>2</sub>) was prepared by the calcination of the PANI@Pt/CNTs at 325 °C in N<sub>2</sub>.

### 1.4 Characterization

An X-ray diffractometer (Bruker D8 Advance diffractometer, Germany) with Cu K $\alpha$  radiation ( $\lambda = 1.5406 \text{ \AA}$ ) was employed to characterize the crystallinity of the samples. X-ray photoelectron spectra (XPS) were obtained on a Thermo Fisher Nexsa XPS spectrometer (USA) with an Al K $\alpha$  radiation at 12 kV. JEOL-JEM 2100F (Japan) transmission electron microscopy (TEM) equipped with an energy dispersive X-ray (EDX) spectrometer at an acceleration voltage of 200 kV was used to obtain TEM images of the samples. The elemental compositions of the samples were determined by inductively coupled plasma optical emission spectra (ICP-OES) using the spectrometer of the Thermo Fisher iCAP 7200 Duo (USA). The thermogravimetal analysis (TGA) was carried out on an American PerkinElmer-STA6000 EXSTAR TG/DTA 6300 apparatus with a ramping rate of 10 °C min<sup>-1</sup> under air. The X-ray absorption spectroscopy (XAS) measurements were conducted with Si(111) crystal monochromators at the BL14W1 beamlines using the Shanghai Synchrotron Radiation Facility

(Shanghai, China). A transmission mode was used to collect the X-ray absorption near edge structure (XANES) and extended X-ray absorption fine structure (EXAFS) spectra using a 4-channel Silicon Drift Detector (SDD) Bruker 5040 at room temperature. The obtained data were processed and analyzed using the software codes Athena and Artemis.<sup>1</sup>

### 1.5 Electrochemical measurements

A CHI 760E workstation using a standard three-electrode cell was utilized to evaluate the HER activities of the samples. A carbon rod served as the counter electrode. Hg/Hg<sub>2</sub>SO<sub>4</sub>, Ag/AgCl, and Hg/HgO were employed as the reference electrodes in the acidic (0.5 M H<sub>2</sub>SO<sub>4</sub>), neutral (1.0 M PBS), and alkaline (1.0 M KOH) media, respectively. The catalyst ink was prepared by dispersing the catalyst (4.0 mg) in 1.0 mL of isopropanol containing 20.0 μL of Nafion solution (5.0%, Sigma-Aldrich) by ultrasonication. A catalyst loaded glassy carbon (GC, 5.0 mm in diameter) was used as the working electrode. Before use, the GC electrode was carefully polished with 0.05 μm Al<sub>2</sub>O<sub>3</sub> powder and rinsed with water. The working electrode was prepared by drop-casting the catalyst ink onto the GC electrode and drying naturally at the ambient temperature. The catalyst mass loading was determined to be ~0.2 mg cm<sup>-2</sup>. Linear sweep voltammograms (LSVs) were recorded at a scan rate of 5.0 mV s<sup>-1</sup>. Electrochemical impedance spectra (EISs) were obtained within the frequency range of 10<sup>5</sup> Hz to 10<sup>-2</sup> Hz. The LSVs reported in this work were calibrated against the reversible hydrogen electrode (RHE) and IR-corrected. The Ohmic resistance is corrected using the following equation:

$$E = E_{\text{RHE}} - I \times R \quad (\text{S1})$$

where E represents the potential corrected for IR drop, E<sub>RHE</sub> denotes the measured potential with respect to the reversible hydrogen electrode (RHE), I is the measured current (prior to background correction), and R stands for the uncompensated resistance determined through electrochemical impedance spectroscopy (EIS) or current-interrupt methods.<sup>2-4</sup>

The long-term stability of the catalyst was evaluated using the RuIr/TiO<sub>2</sub> loaded carbon paper (CP) with a mass loading of 2.0 mg cm<sup>-2</sup> as the counter electrode to avoid the problem of the carbon electrode corrosion in the extended period.

The electrochemical surface area (ECSA) was evaluated from the cyclic voltammetry (CV) between +0.05 and +0.40 V.

$$\text{ECSA} = Q/\Gamma m \quad (\text{S2})$$

where Q is the transferred charge,  $\Gamma$  is the specific charge (210  $\mu\text{C cm}^{-2}$ ) of a hydrogen monolayer on polycrystalline Pt surface, m is the mass of Pt on the GCE.<sup>5</sup>

For CO stripping test, the potential of the working electrode was maintained at 0.05 V vs. RHE while CO was bubbled into 0.5 M H<sub>2</sub>SO<sub>4</sub>, 1.0 M PBS, and 1.0 M KOH for 30 min, respectively. The dissolved CO was then removed by bubbling the electrolytes with N<sub>2</sub> for 30 min. Stripping measurements were initiated from 0.05 V vs. RHE and first scanned in the anodic direction at 20.0 mV s<sup>-1</sup> for at least two consecutive cycles.

### 1.6 Turnover frequency (TOF)

The underpotential copper deposition (Cu<sub>upd</sub>) was performed to quantify the actual surface area of the Pt NPs exposed for the catalytic reactions in the acidic media. Specifically, the Cu<sub>upd</sub> was carried out in an aqueous solution with 0.1 M H<sub>2</sub>SO<sub>4</sub> and 2.0 mM CuSO<sub>4</sub>. Before the data collection, the CVs were performed in 0.1 M H<sub>2</sub>SO<sub>4</sub> until a stable voltammogram was achieved. The electrode was subsequently transferred to the solution of 0.1 M H<sub>2</sub>SO<sub>4</sub> + 2.0 mM CuSO<sub>4</sub> and polarized at 0.3 V vs. RHE for 100 s. The Cu<sub>upd</sub> was carried out from 0.3 V to 1.4 V vs. RHE at a scan rate of 20.0 mV s<sup>-1</sup>.

After correcting for the charge consumed in the double-layer capacitance (obtained via CV scanning in 0.1 M H<sub>2</sub>SO<sub>4</sub> without any copper ions), the peak area corresponding to the Cu stripping was integrated. The charge consumed for the deposition of a monolayer of Cu (Q<sub>Cu<sub>upd</sub></sub>) was then determined using a conversion factor of 0.42 mC cm<sup>-2</sup>.<sup>6</sup> The electrochemical

active surface area of the catalyst based on the  $\text{Cu}_{\text{upd}}$  ( $S_{\text{upd}}$ ) was then obtained using the following equation:

$$S_{\text{upd}} = Q_{\text{Cu}_{\text{upd}}} / 0.42 \quad (\text{S3})$$

Based on the  $S_{\text{upd}}$ , the exact number of the Pt atoms exposed can be estimated by the following formula:

$$\text{TOF} = \frac{\text{Total hydrogen turnovers per geometric area}}{\text{Number of Pt sites}} \quad (\text{S4})$$

Total hydrogen turnovers per geometric area

$$= |j| \frac{\text{mA}}{\text{cm}^2} \times \frac{1 \frac{\text{C}}{\text{s}}}{1000 \text{ mA}} \times \frac{1 \text{ mol e}^-}{96485 \text{ C}} \times \frac{1 \text{ mol H}_2}{2 \text{ mol e}^-} \times \frac{6.022 \times 10^{23} \text{ mol H}_2}{1 \text{ mol H}_2}$$

$$= 3.12 \times 10^{15} |j| \text{ H}_2 \text{ s}^{-1} \text{ per mA cm}^{-2}$$

$$\text{Number of Pt sites} = 1.71 \times 10^{15} \text{ atoms cm}^{-2} \times A_{\text{ECSA}}$$

## 1.7 Overall water splitting

The overall water splitting was performed using the C@Pt/CNTs-325 as the cathode catalyst of a water electrolyzer, where the commercial RuIr/TiO<sub>2</sub> served as the anode catalyst. The cathodic electrode was prepared by drop-casting a homogeneous catalyst ink onto carbon paper and allowing it to dry naturally. The catalyst ink was prepared by dispersing 8.0 mg of the catalyst and 40.0  $\mu\text{L}$  of 5.0 wt.% Nafion solution in 1.0 mL of isopropanol, followed by sonication. The mass loading of the catalyst was controlled at 4.0  $\text{mg cm}^{-2}$ . Additionally, the chronopotentiometric curves were recorded at a constant current density of 1.0  $\text{A cm}^{-2}$ .

## 1.8 DFT calculations

The dipole-corrected DFT calculations were done with the Vienna ab-initio simulation package (VASP).<sup>7</sup> The generalized gradient approximation (GGA) in the form of the Perdew-Burke-Ernzerhof (PBE) was utilized to describe electron-electron exchange correlations.<sup>8</sup> The electron-ion interactions were performed using the projector augment wave (PAW) type pseudopotential.<sup>9</sup> The cut-off energy was set at 450 eV for plane-wave expansion. The

convergence criteria for energy and force were set at  $1 \times 10^{-5}$  eV and  $0.02$  eV  $\text{\AA}^{-1}$ , respectively. The  $\Gamma$ -centered k-point mesh was sampled for the Brillouin zone for both the cell and slab optimization. Specifically, the k-points were selected to ensure  $a_n \times k_n$  ( $n = 1, 2, 3$ )  $> 30$   $\text{\AA}$  ( $a_n$  is the lattice parameters of the cell and slab). Calculations of the HER energetics were conducted on the (111) surface of the cubic structure of Pt. The van der Waals corrections were done using DFT-D2 method.<sup>10</sup> A vacuum slab of  $> 18$   $\text{\AA}$  in z-direction was added to avoid the artificial interactions between the periodic images. The hydrogen adsorption free energy was computed using the equation:

$$\Delta G_{H^*} = (E_{\text{surface+H}} - E_{\text{surface}}) - 1/2 E_{H_2} + \Delta ZPE - T\Delta S \quad (\text{S5})$$

where  $\Delta ZPE$  and  $\Delta S$  are the difference in the zero-point energy and entropy between the adsorbed H atom and the gaseous phase  $H_2$ . The climbing image nudge band (ci-NEB) method was employed to calculate the energy barrier for the water dissociation.<sup>11</sup>

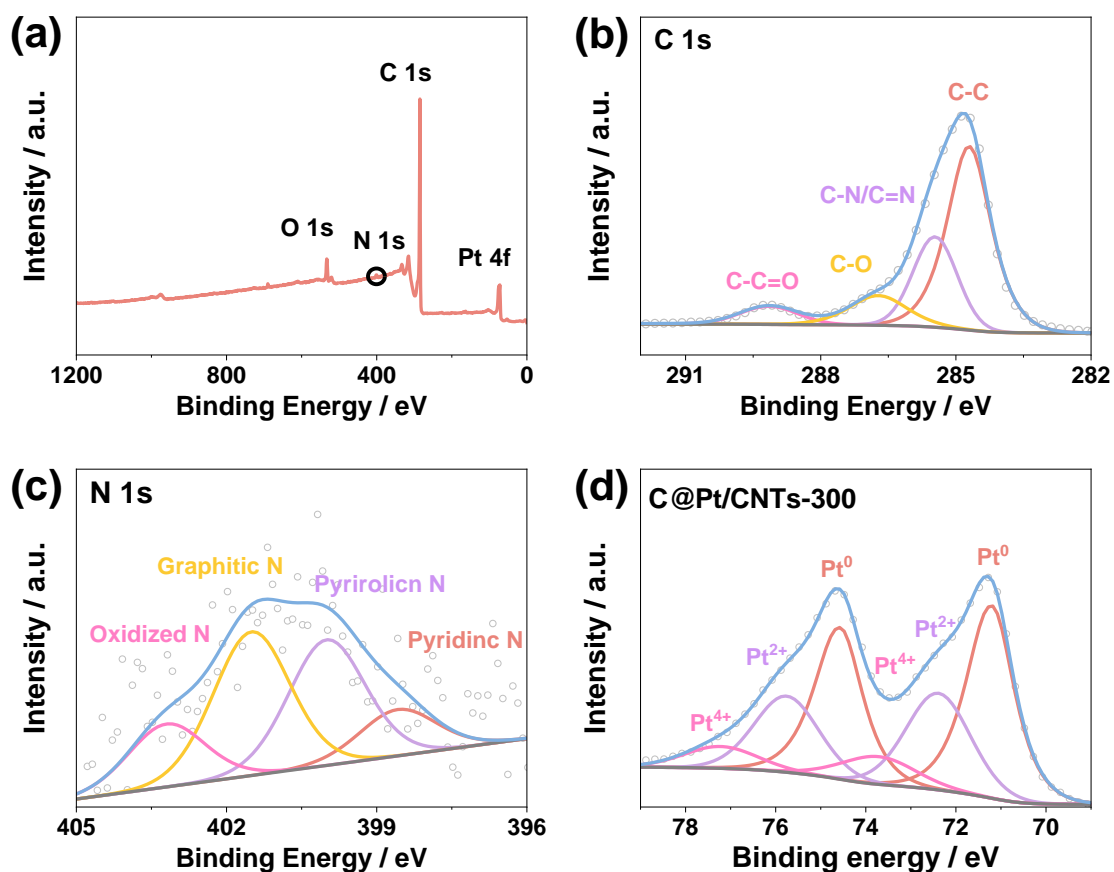


**Figure S1.** (a) XPS survey, (b) C 1s, and (c) N 1s spectra of C@Pt/CNTs-325. (d) Pt 4f spectrum of the C@Pt/CNTs-300.

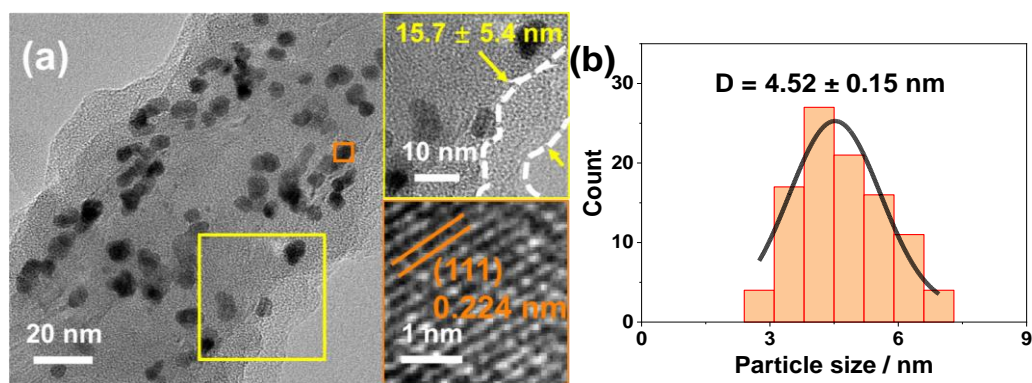


**Figure S2.** (a) TEM image of PANI@Pt/CNTs. The right panel shows the magnified HRTEM (upper) image and lattice fringes (lower) of the Pt NPs. (b) Particle size distribution histogram of the Pt NPs in PANI@Pt/CNTs.

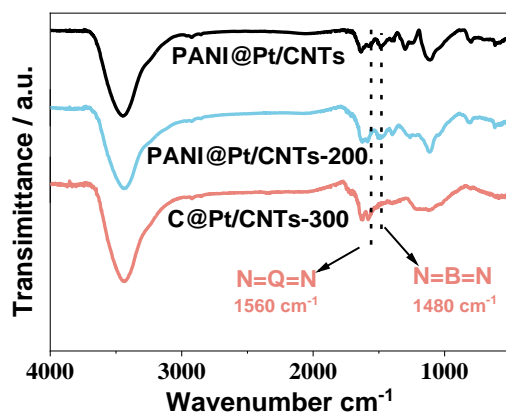


**Figure S3.** FTIR spectra of PANI@Pt/CNTs, PANI@Pt/CNTs-200, and C@Pt/CNTs-300.

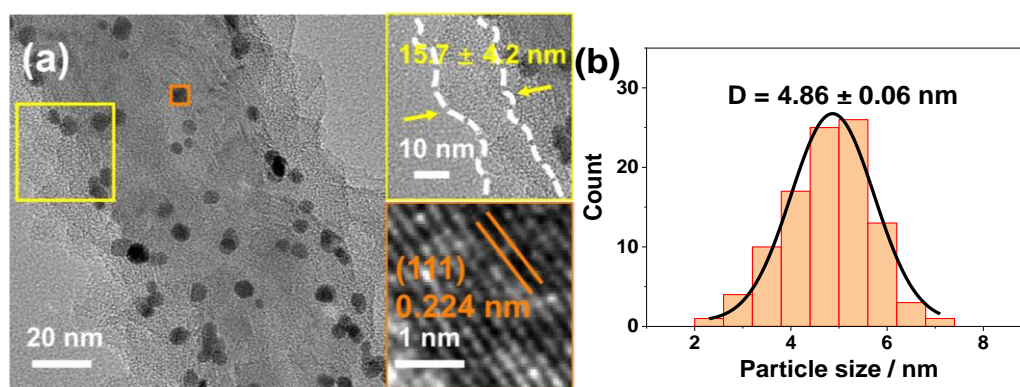


**Figure S4.** (a) TEM image of PANI@Pt/CNTs-200. The right panel shows the magnified HRTEM (upper) image and lattice fringes (lower) of the Pt NPs. (b) Particle size distribution histogram of the Pt NPs in PANI@Pt/CNTs-200.

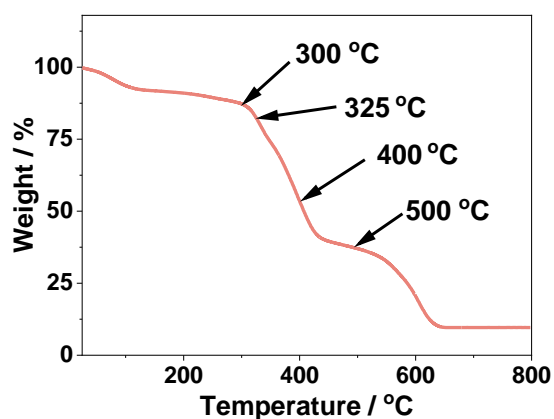


**Figure S5.** TGA curve of PANI@Pt/CNTs.

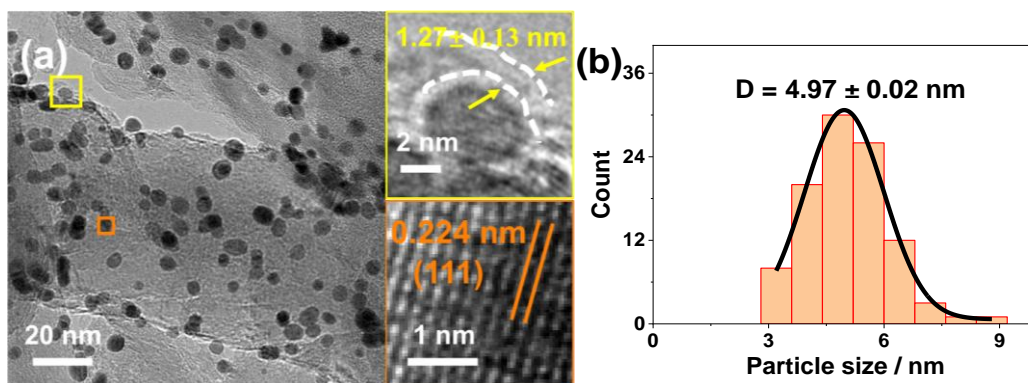


**Figure S6.** (a) TEM image of C@Pt/CNTs-300. The right panel shows the magnified HRTEM (upper) image and lattice fringes (lower) of the Pt NPs. (b) Particle size distribution histogram of the Pt NPs in C@Pt/CNTs-300.

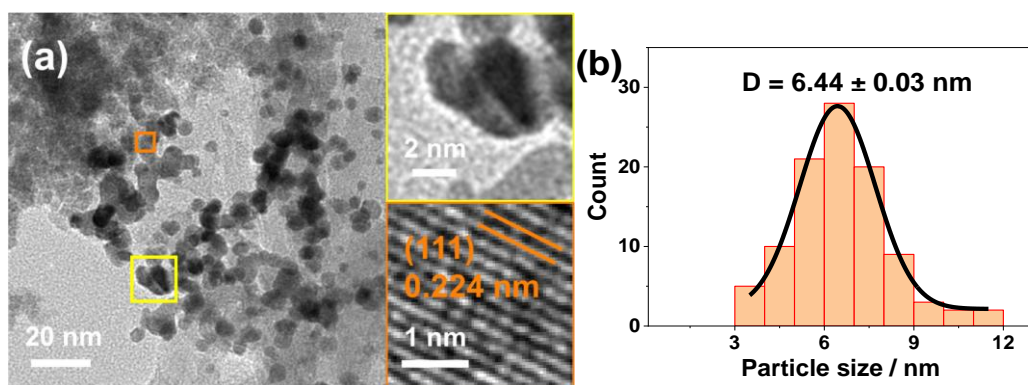


**Figure S7.** (a) TEM image of Pt/CNTs-400. The right panel shows the magnified HRTEM (upper) image and lattice fringes (lower) of the Pt NPs. (b) Particle size distribution histogram of the Pt NPs in Pt/CNTs-400.

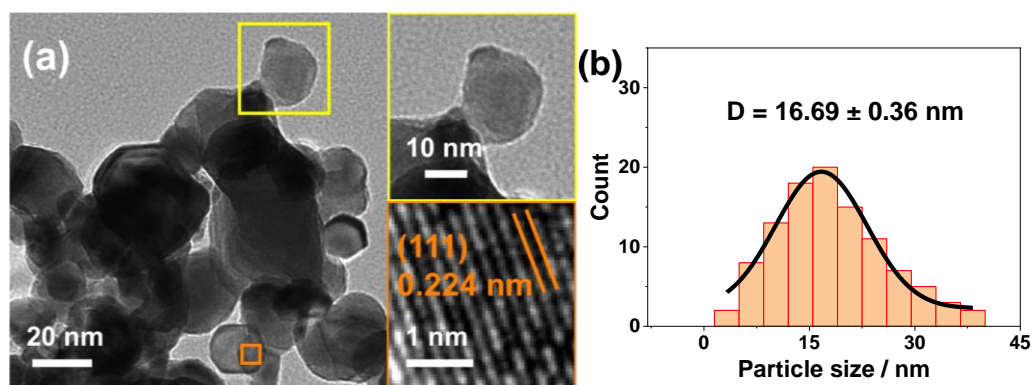


**Figure S8.** (a) TEM image of Pt-500. The right panel shows the magnified HRTEM (upper) image and lattice fringes (lower) of the Pt NPs. (b) Particle size distribution histogram of the Pt NPs in Pt-500.

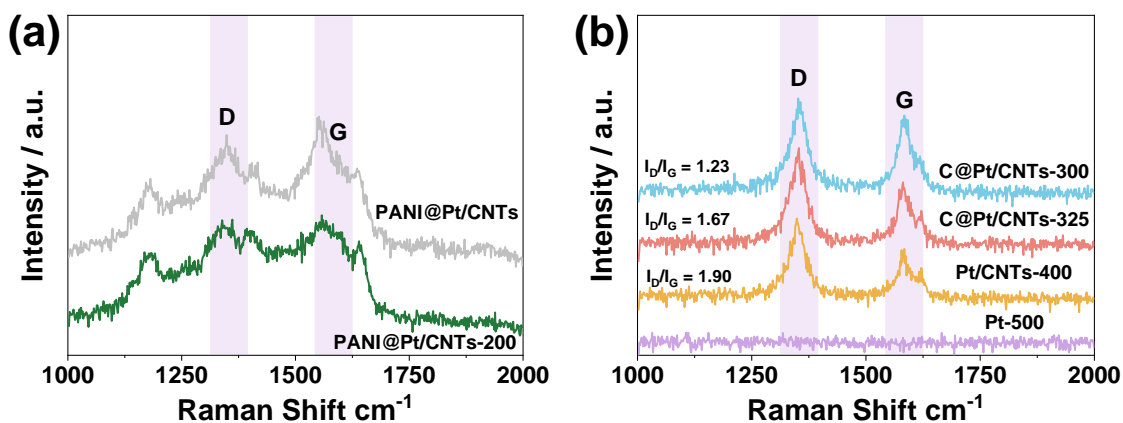


**Figure S9.** (a) Raman spectra of PANI@Pt/CNTs and PANI@Pt/CNTs-200. (b) Raman spectra of C@Pt/CNTs-300, C@Pt/CNTs-325, Pt/CNTs-400 and Pt-500.

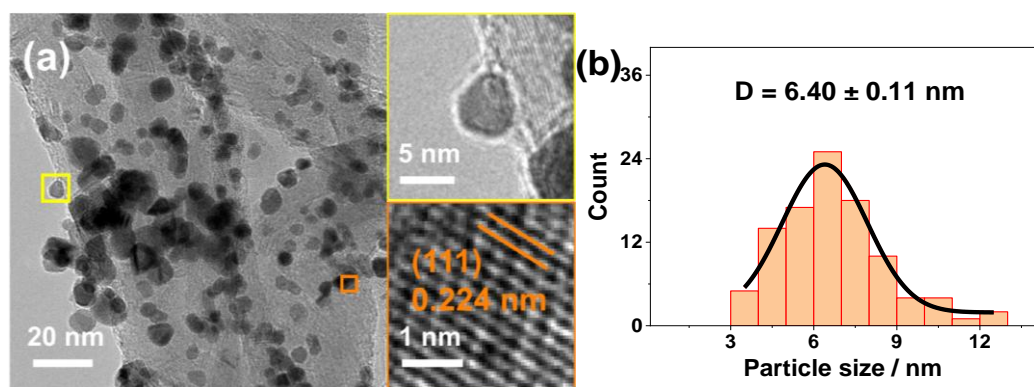


**Figure S10.** (a) TEM image of Pt/CNTs-325. The right panel shows the magnified HRTEM (upper) image and lattice fringes (lower) of the Pt NPs. (b) Particle size distribution histogram of the Pt NPs in Pt/CNTs-325.

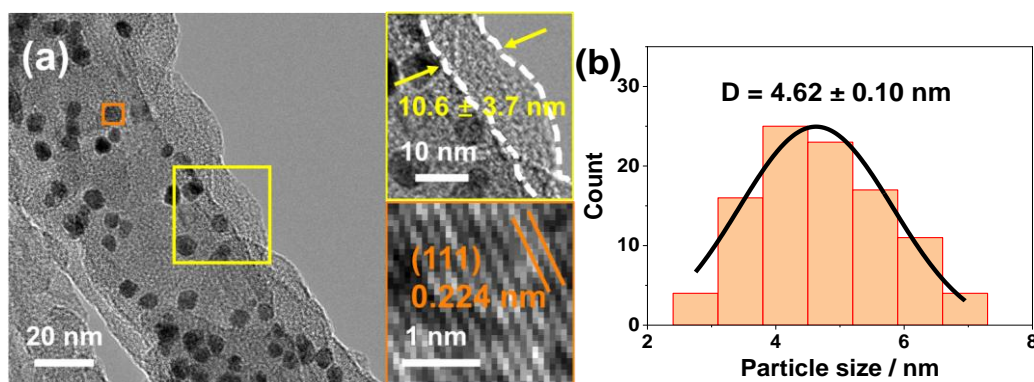


**Figure S11.** (a) TEM image of C@Pt/CNTs-325(N<sub>2</sub>). The right panel shows the magnified HRTEM (upper) image and lattice fringes (lower) of the Pt NPs. (b) Particle size distribution histogram of the Pt NPs in C@Pt/CNTs-325(N<sub>2</sub>).

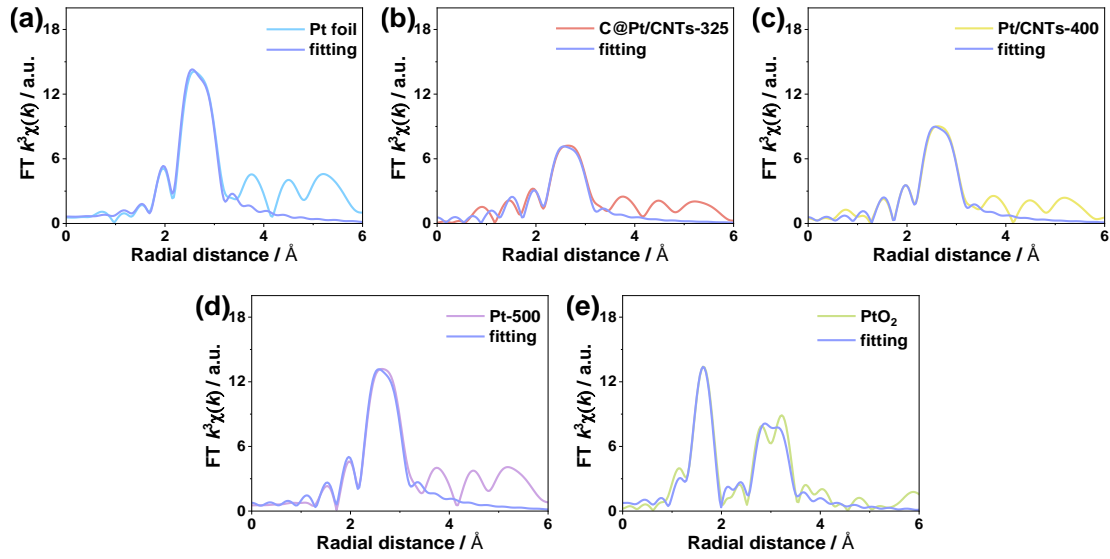


**Figure S12.** EXAFS fitting curve of (a) Pt foil, (b) C@Pt/CNTs-325, (c) Pt/CNTs-400, (d) Pt-500, and (e) PtO<sub>2</sub> in R-space.

**Table S1.** FT-EXAFS fitting results of C@Pt/CNTs-325, Pt/CNTs-400, and Pt-500 using the Pt foil and PtO<sub>2</sub> as the references.

Sample	Shell	CN	R(Å)	$\sigma^2$	$\Delta E_0$	R factor
Pt foil	Pt-Pt	12.00	2.76	0.005	7.17	0.0085
C@Pt/CNTs-325	Pt-C	0.50	1.75	0.015	7.16	0.0155
	Pt-O	2.09	1.97	0.015		
	Pt- Pt	5.89	2.76	0.004		
Pt/CNTs-400	Pt-C	0.20	1.75	0.015	7.06	0.0042
	Pt-O	1.41	1.97	0.011		
	Pt-Pt	7.07	2.76	0.005		
Pt-500	Pt-O	1.23	1.97	0.015	7.05	0.010
	Pt-Pt	9.49	2.76	0.004		
PtO <sub>2</sub>	Pt-O	6.00	2.01	0.003	9.59	0.0172
	Pt-O-Pt	9.36	3.11	0.005		

CN: coordination numbers of identical atoms;

R: interatomic distance;

$\sigma^2$ : Debye-Waller factors;

$\Delta E_0$ : energy shift. R factor: goodness of fit.

$S_0^2$  was set to 0.89, according to the experimental EXAFS fit of Pt foil reference by fixing CN as the known crystallographic value.

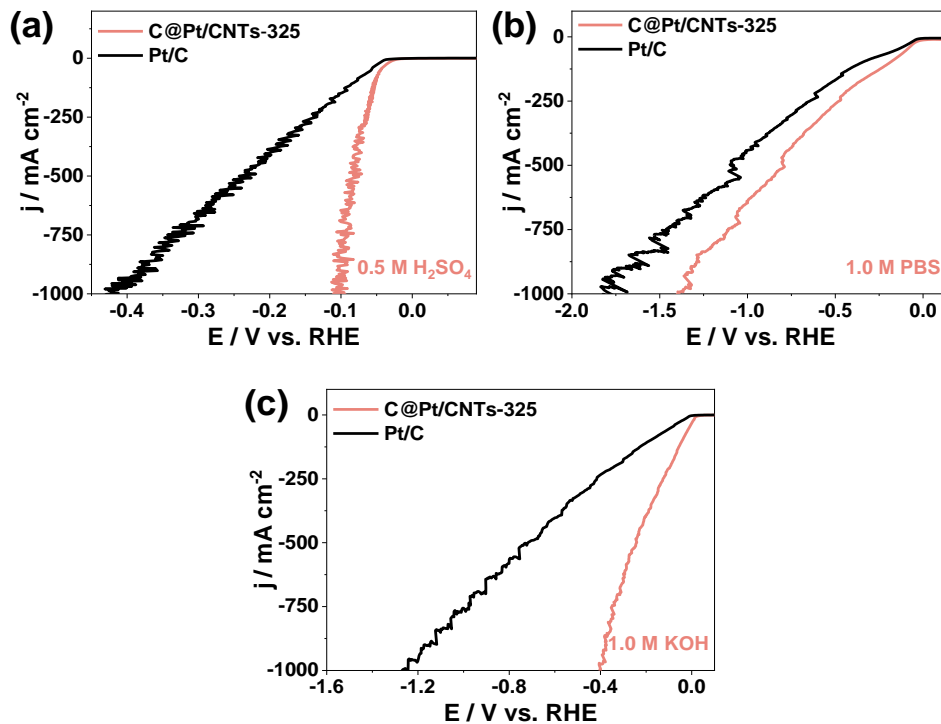


**Figure S13.** HER polarization curves of C@Pt/CNTs-325 and Pt/C in (a) 0.5 M  $\text{H}_2\text{SO}_4$ , (b) 1.0 M PBS, and (c) 1.0 M KOH.

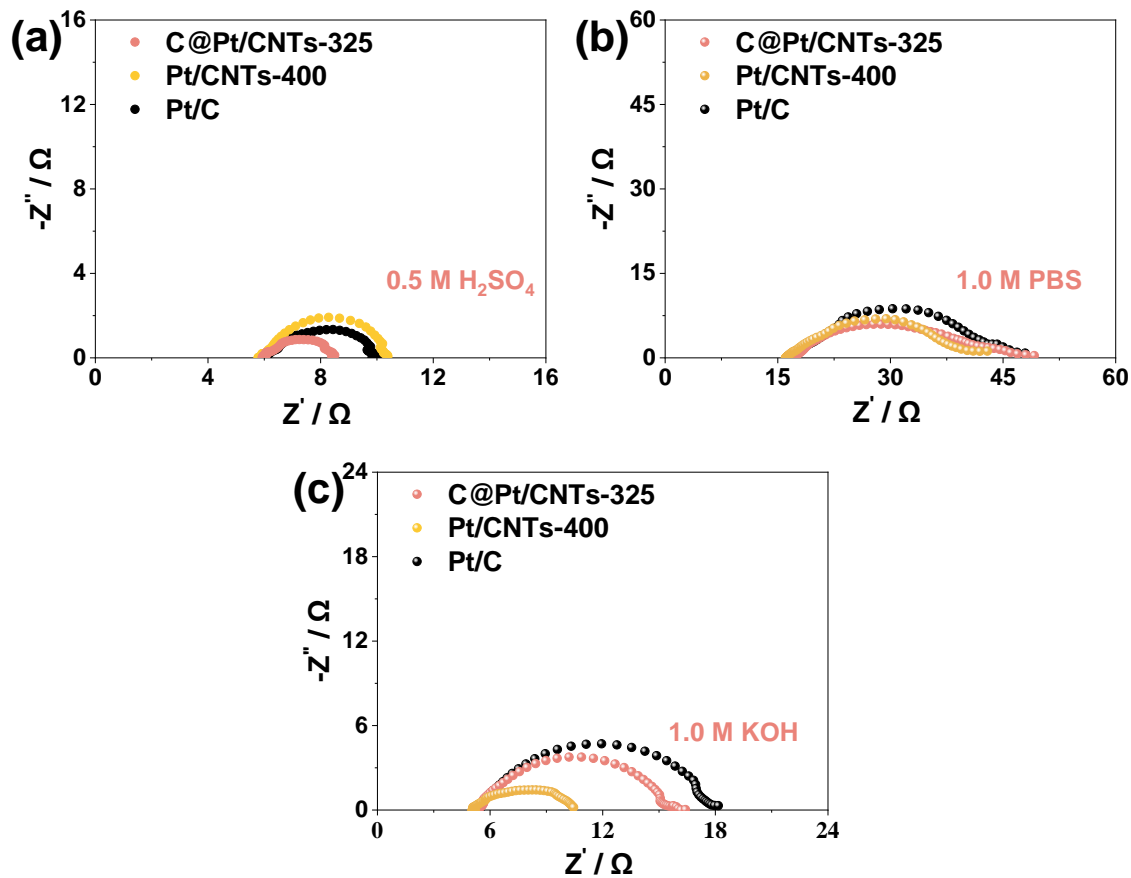


**Figure S14.** EIS spectra of C@Pt/CNTs-325, Pt/CNTs-400, and Pt/C in (a) 0.5 M  $\text{H}_2\text{SO}_4$ , (b) 1.0 M PBS, and (c) 1.0 M KOH.

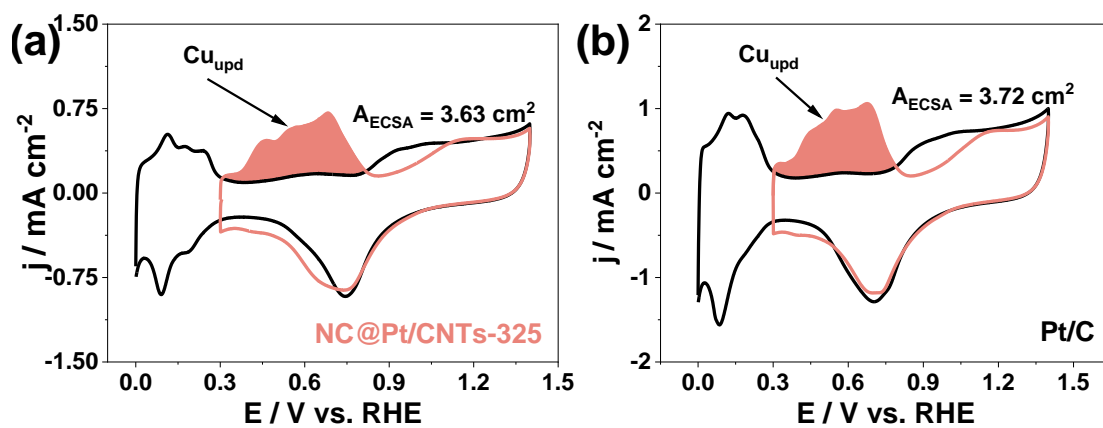


**Figure S15.** CVs in the solutions of 0.1 M  $\text{H}_2\text{SO}_4$  (black) and 0.1 M  $\text{H}_2\text{SO}_4$  + 2.0 mM  $\text{CuSO}_4$  (red) for (a) C@Pt/CNTs-325, (b) Pt/C.

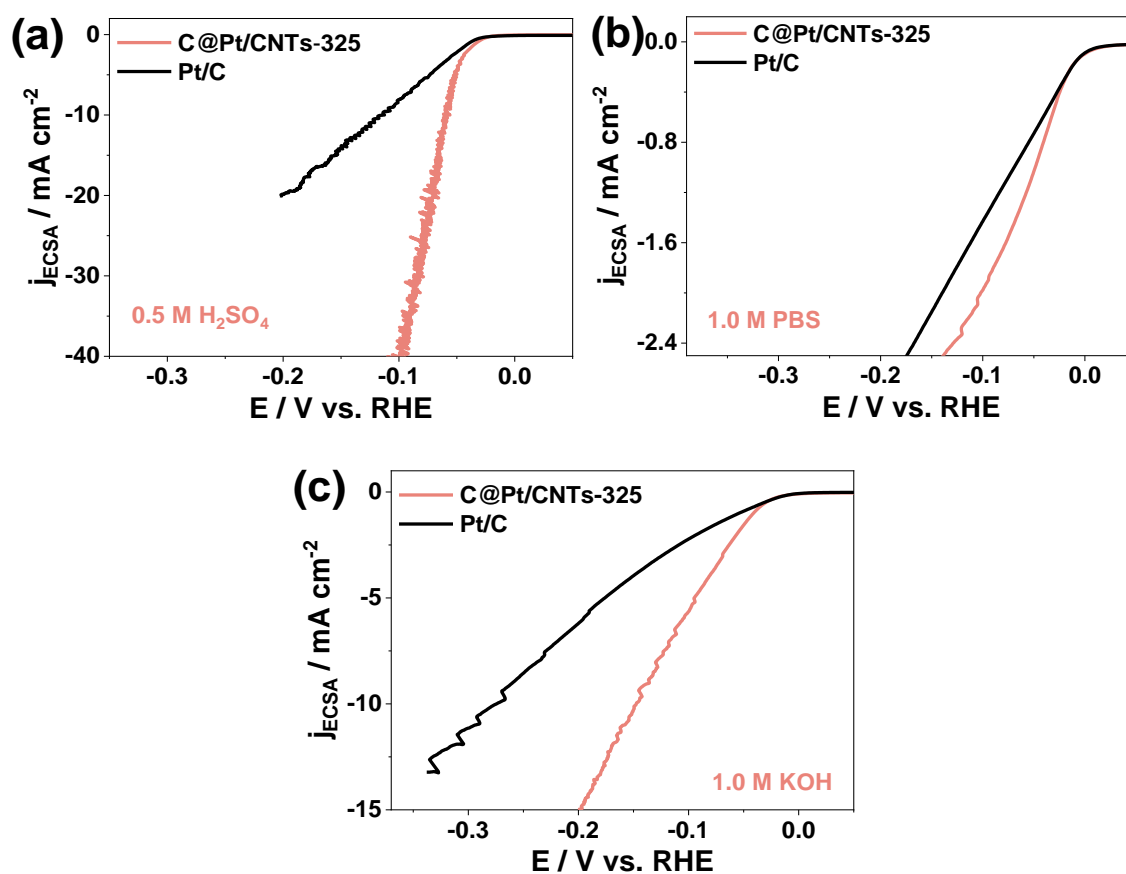


**Figure S16.** ECSA-normalized LSV curves of C@Pt/CNTs-325 and Pt/C in (a) 0.5 M  $\text{H}_2\text{SO}_4$ , (b) 1.0 M PBS, and (c) 1.0 M KOH.

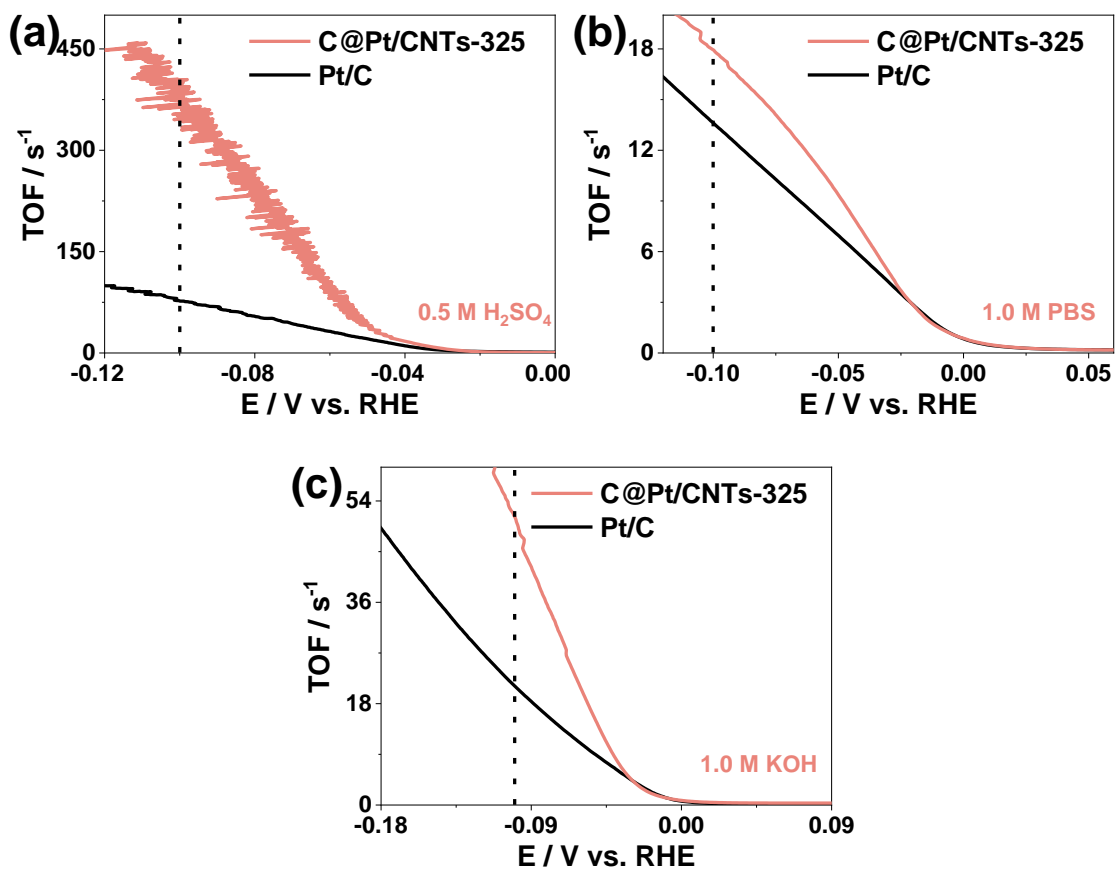


**Figure S17.** TOFs of C@Pt/CNTs-325 and Pt/C in (a) 0.5 M  $\text{H}_2\text{SO}_4$ , (b) 1.0 M PBS, and (c) 1.0 M KOH.

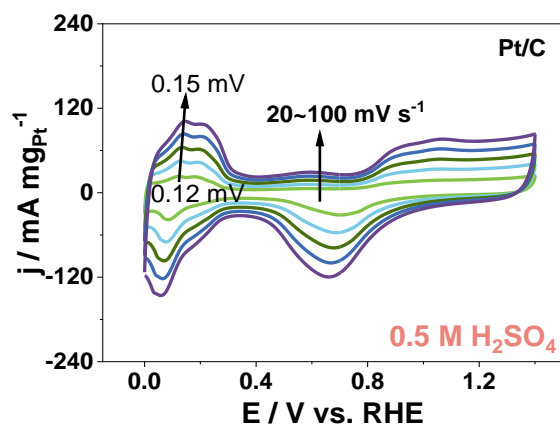


**Figure S18.** CVs of Pt/C at the different scan rates in the acidic media.

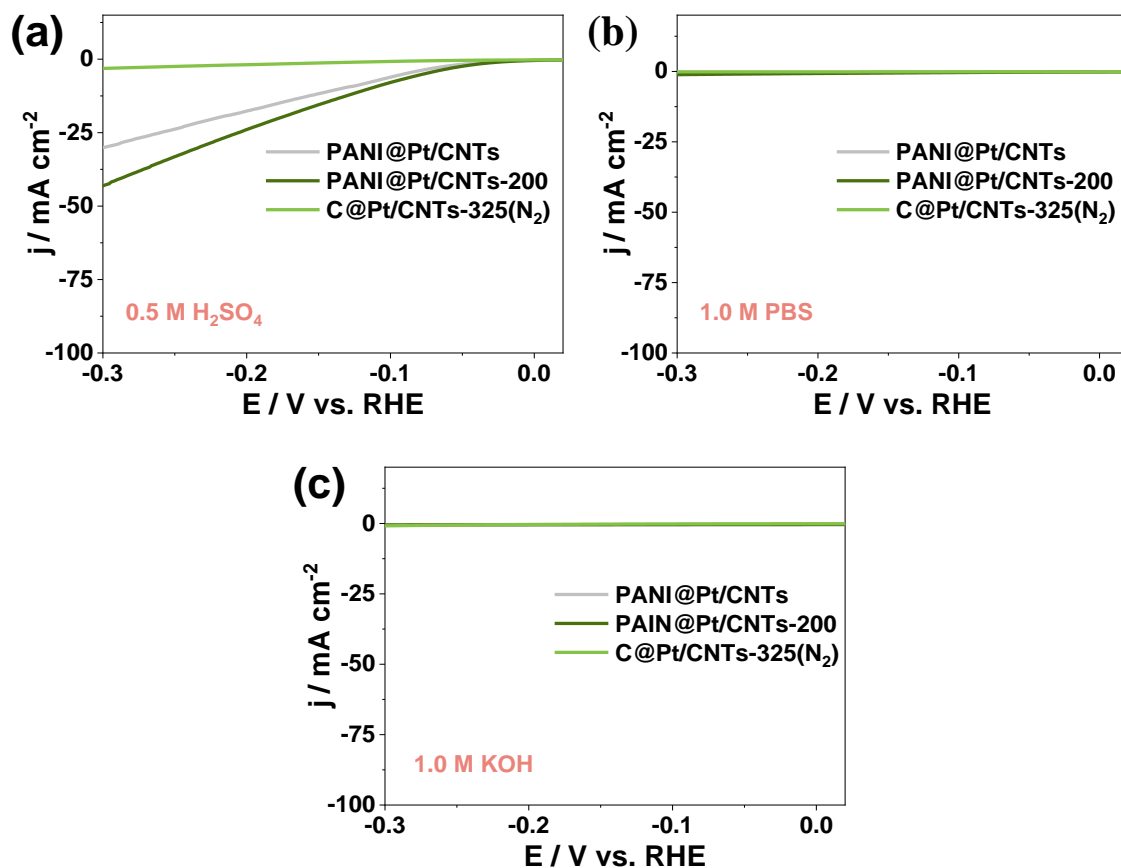


**Figure S19.** HER polarization curves of PANI@Pt/CNTs, PANI@Pt/CNTs-200, and C@Pt/CNTs-325(N<sub>2</sub>) in the (a) acidic, (b) neutral, and (d) alkaline media.

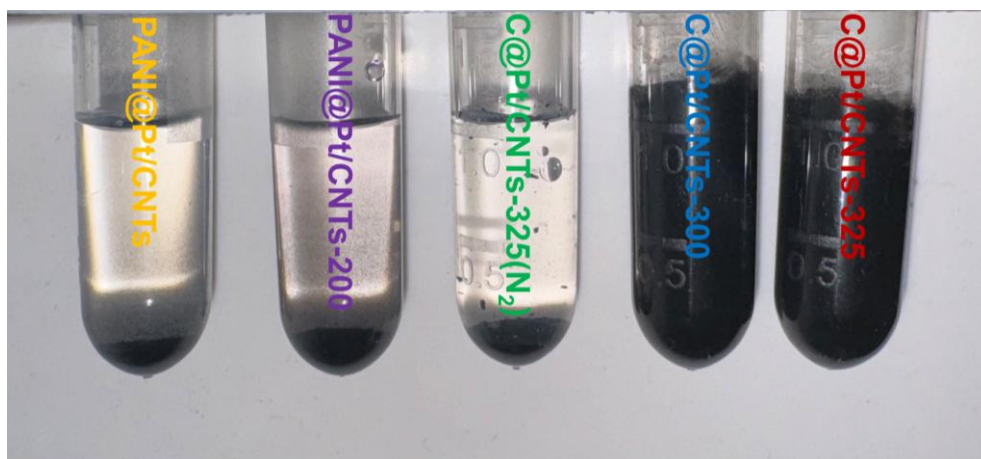


**Figure S20.** Photograph of PANI@Pt/CNTs, PANI@Pt/CNTs-200, C@Pt/CNTs-325(N<sub>2</sub>), C@Pt/CNTs-300, and C@Pt/CNTs-325 dispersion in water.

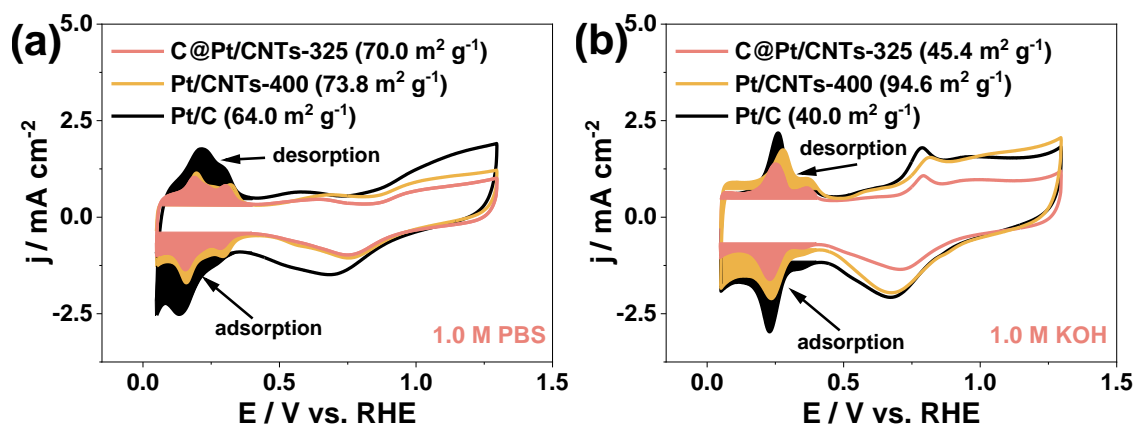


**Figure S21.** CVs of C@Pt/CNTs-325, Pt/CNTs-400, and Pt/C in (a) 1.0 M PBS and (b) 1.0 M KOH.

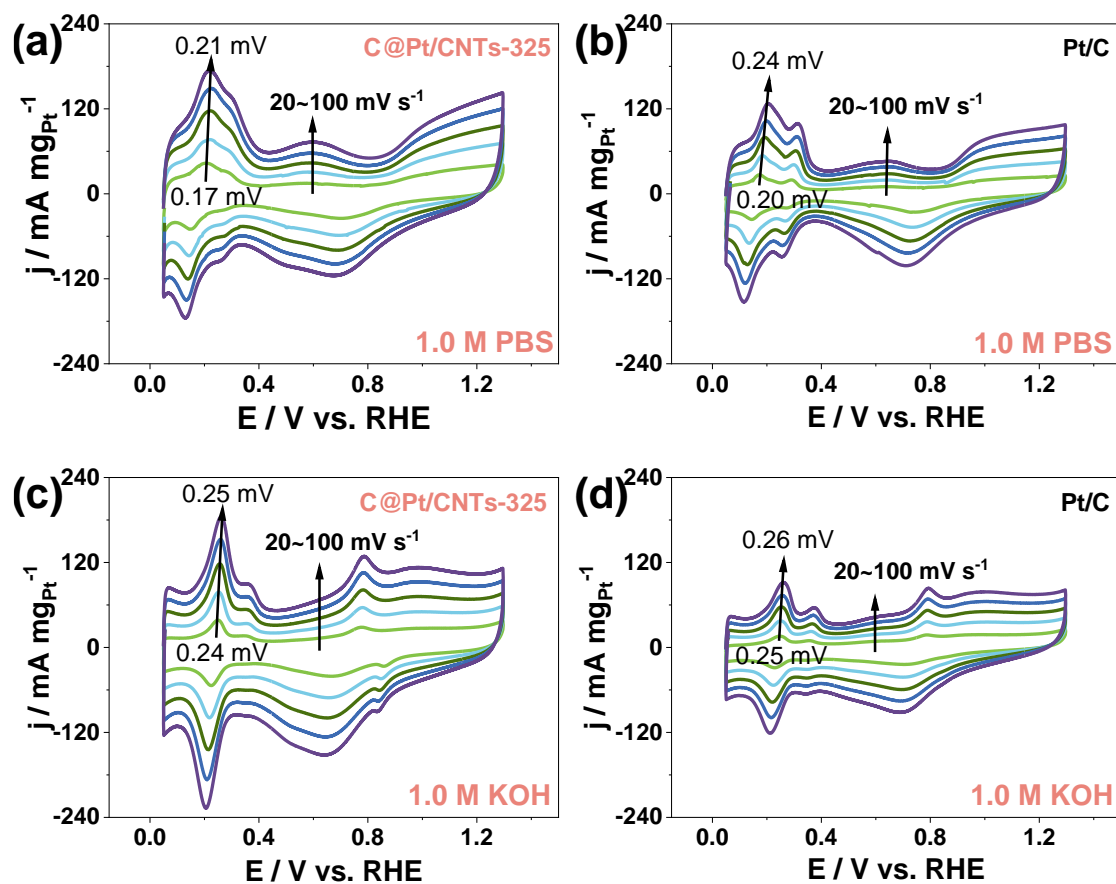


**Figure S22.** CVs of (a) C@Pt/CNTs-325 and (b) Pt/C in the neutral media. CVs of (c) C@Pt/CNTs-325 and (d) Pt/C in the alkaline media.

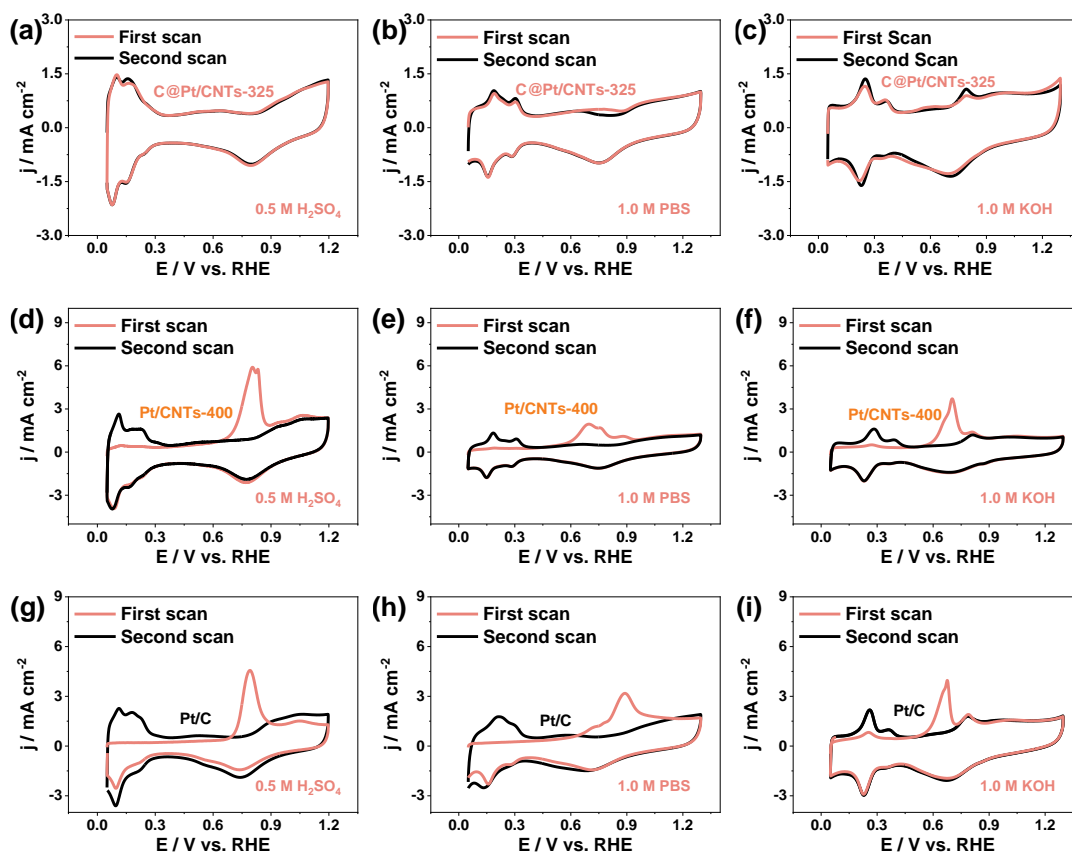


**Figure S23.** CO stripping of C@Pt/CNTs-325, Pt/CNTs-400, and Pt/C in 0.5 M H<sub>2</sub>SO<sub>4</sub>, 1.0 M PBS and 1.0 M KOH.

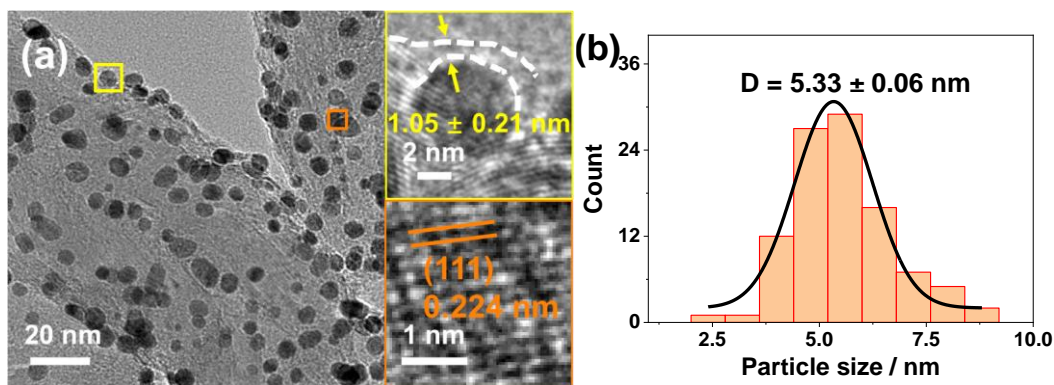


**Figure S24.** (a) TEM image of C@Pt/CNTs-325 after HER in 0.5 M H<sub>2</sub>SO<sub>4</sub>. The right panel shows the magnified HRTEM (upper) image and lattice fringes (lower) of the Pt NPs. (b) Particle size distribution histogram of the Pt NPs in C@Pt/CNTs-325 after HER in 0.5 M H<sub>2</sub>SO<sub>4</sub>.

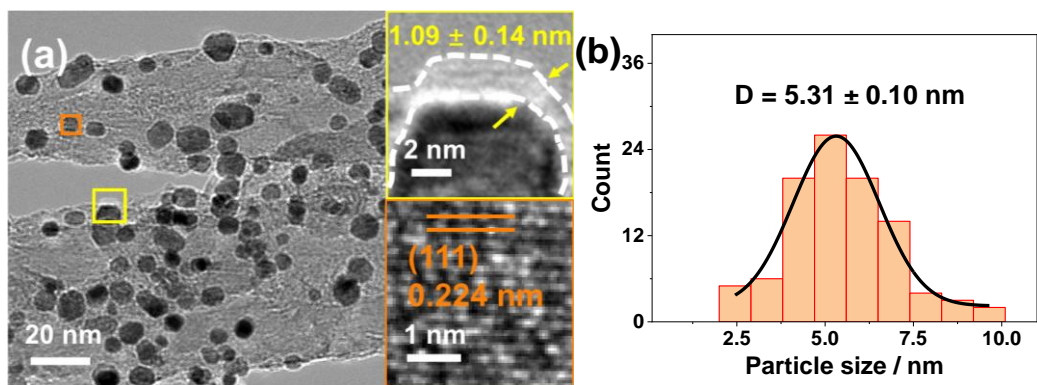


**Figure S25.** (a) TEM image of C@Pt/CNTs-325 after the HER in 1.0 M PBS. The right panel shows the magnified HRTEM (upper) image and lattice fringes (lower) of the Pt NPs. (b) Particle size distribution histogram of the Pt NPs in C@Pt/CNTs-325 after HER in 1.0 M PBS.

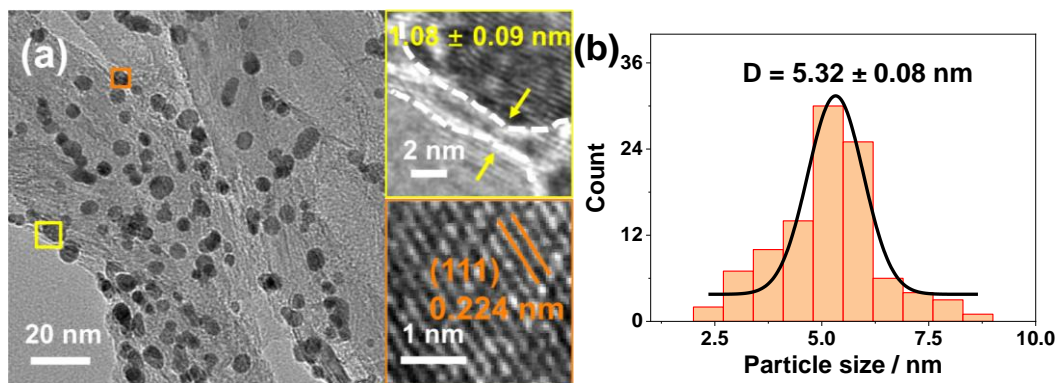


**Figure S26.** (a) TEM image of C@Pt/CNTs-325 after the HER in 1.0 M KOH. The right panel shows the magnified HRTEM (upper) image and lattice fringes (lower) of the Pt NPs. (b) Particle size distribution histogram of the Pt NPs in C@Pt/CNTs-325 after HER in 1.0 M KOH.

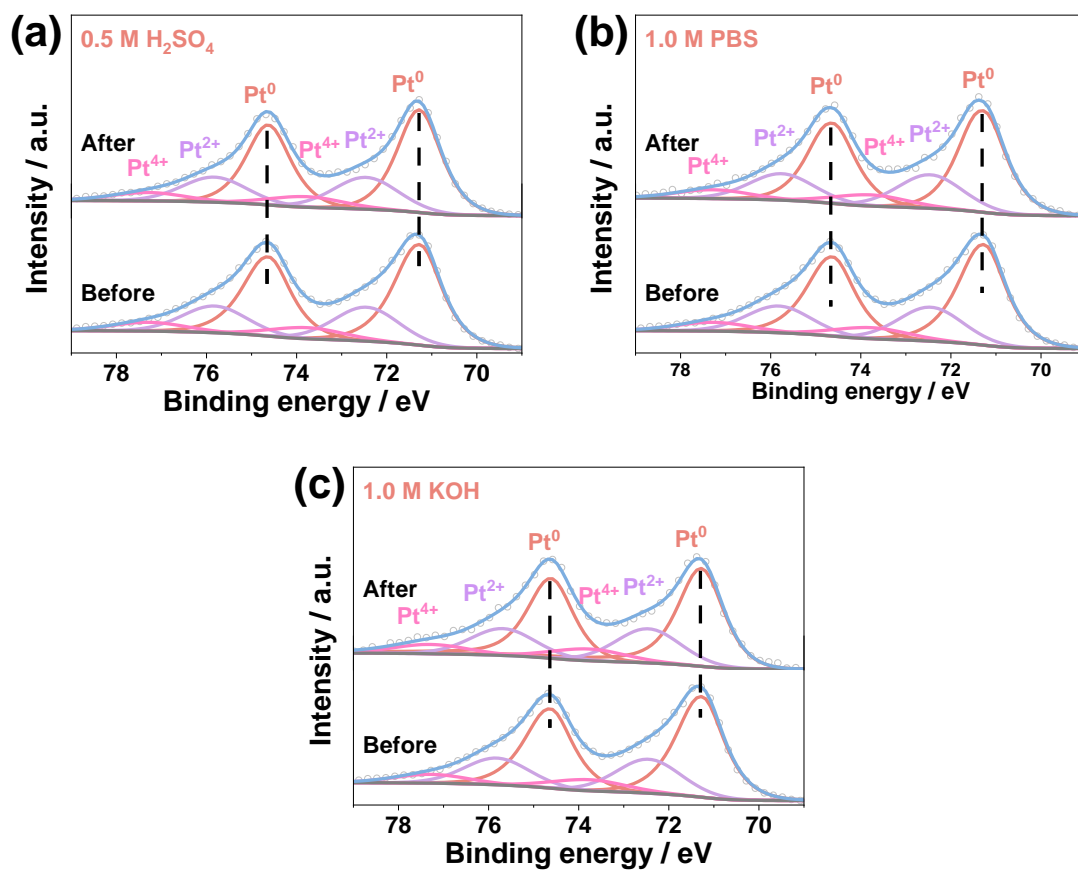


**Figure S27.** Pt 4f spectra of C@Pt/CNTs-325 before and after the HER in the (a) acidic, (b) neutral, and (c) alkaline media.

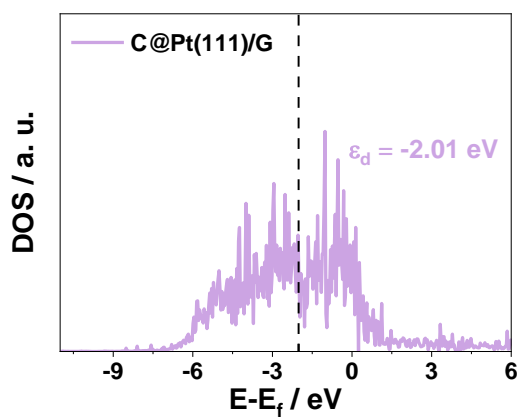


**Figure S28.** PDOS spectrum of C@Pt(111)/G.

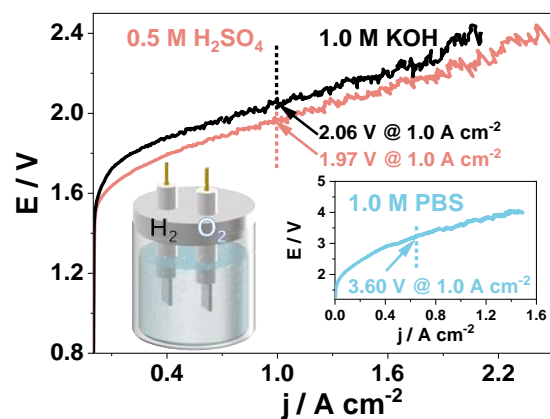


**Figure S29.** Polarization curves of Pt/C||RuIr/TiO<sub>2</sub> for overall water splitting in the acid, neutral, and alkaline media.

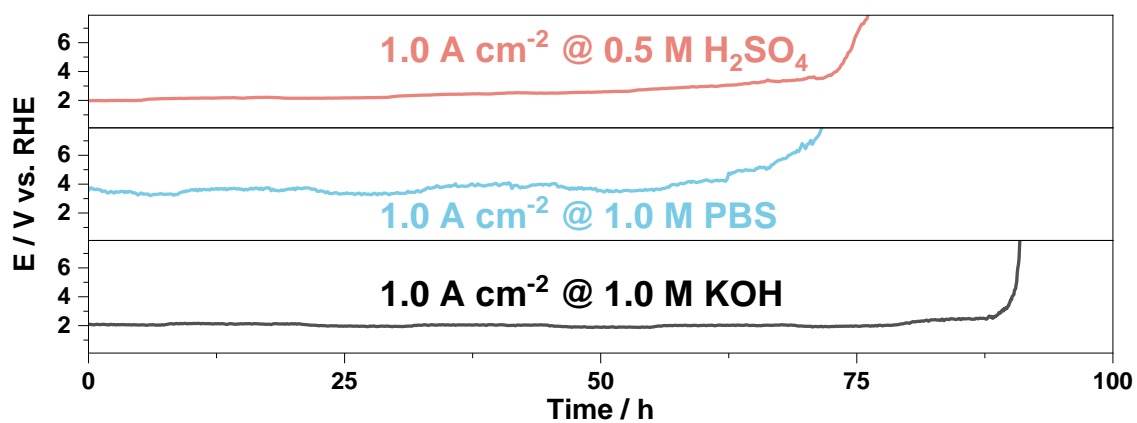


**Figure S30.** Chronopotentiometric curves of Pt/C||RuIr/TiO<sub>2</sub> for overall water splitting in the acid, neutral, and alkaline media at 1.0 A cm<sup>-2</sup>.

**Table S2.** HER performance comparison of C@Pt/CNTs-325 ( $\eta_{10}$ ) with those reported.

Catalyst	Mass loading (mg cm <sup>-2</sup> )	Electrolyte	$\eta_{10}$ (mV)	Tafel slope (mV dec <sup>-1</sup> )	Stability	Ref.
C@Pt/CNTs-325	0.20	0.5 M H <sub>2</sub> SO <sub>4</sub>	27.4	30.6	>600 h (1.0 A cm <sup>-2</sup> )	This work
		1.0 M PBS	30.3	36.3		
		1.0 M KOH	31.1	34.9		
Pt-TiO <sub>2-x</sub> NSs	0.20	0.5 M H <sub>2</sub> SO <sub>4</sub>	36.0	32.1	50 h (100.0 mV)	12
		1.0 M PBS	87.0	67.6		
		1.0 M KOH	69.0	50.2		
Pt <sub>3</sub> Ni <sub>2</sub> NWS-S/C	\	1.0 M KOH	42.0	/	5 h (5.0 mA cm <sup>-2</sup> )	13
		Pt@CoO <sub>x</sub>	1.0 M PBS	82.0	51.5	24 h (10.0 mA cm <sup>-2</sup> )
Pt-Co(OH) <sub>2</sub> /CC	6.9	1.0 M PBS	84.0	/	1000 cycles	15
		1.0 M KOH	32.0	70.0		
Pt/NiRu-OH	0.16	1.0 M KOH	38.0	39.0	5000 cycles	16
Pt SAs/MoS <sub>2</sub>	\	0.5 M H <sub>2</sub> SO <sub>4</sub>	44.0	34.8	20 h (50.0 mV)	17
		1.0 M KOH	123.0	76.7		
PtSe <sub>2</sub> /Pt	~0.35	1.0 M KOH	42.0	53.0	48 h (10.0 mA cm <sup>-2</sup> )	18
		Pt/MoS <sub>2</sub> -NTA/Ti <sub>3</sub> C <sub>2</sub>	0.5 M H <sub>2</sub> SO <sub>4</sub>	32.0		
CDs/Pt-PANI	\	0.5 M H <sub>2</sub> SO <sub>4</sub>	30.0	41.7	\	20
		1.0 M PBS	\	458.0		
		1.0 M KOH	56.0	58.0		
PATP/Pt NPs	\	0.5 M H <sub>2</sub> SO <sub>4</sub>	86.1	66.7	10 h (86.0 mV)	21
		1.0 M PBS	~170.0	\		
PtNi-O	0.04	1.0 M KOH	~149.0	\	10 h (10.0 mA cm <sup>-2</sup> )	22
		0.5 M H <sub>2</sub> SO <sub>4</sub>	30.0	31.0		
$\alpha$ -MoC <sub>1-x</sub> /Pt NPs	2.00	1.0 M KOH	67.0	55.0	50 h (10.0 mA cm <sup>-2</sup> )	23
		1.0 M KOH	44.0	54.2		
Rh@Pt <sub>0.83</sub> NBs	~0.02	1.0 M KOH	44.0	54.2	5000 cycles	24
Pt@Cu-0.3	0.30	1.0 M PBS	35.0	61.0	10 h (100.0 mA cm <sup>-2</sup> )	25
Pt@PCM	\	0.5 M H <sub>2</sub> SO <sub>4</sub>	105.0	65.3	5 h (150.0 mV)	26
		1.0 M KOH	150.0	73.6		
PtCoFe@CN	~0.29	0.5 M H <sub>2</sub> SO <sub>4</sub>	45.0	32.0	10000 cycles	27
		1.0 M KOH	120.0	\		
Ti <sub>3</sub> C <sub>2</sub> T <sub>x</sub> -PtSA	0.10	0.5 M H <sub>2</sub> SO <sub>4</sub>	38.0	45.0	1000 cycles	28
Pt Cs/MoO <sub>2</sub> NSs-L	~0.36	0.5 M H <sub>2</sub> SO <sub>4</sub>	47.0	32.6	12 h (120.0 mA cm <sup>-2</sup> )	29
PtNi@Ti <sub>3</sub> C <sub>2</sub> MXene	0.05	1.0 M KOH	36.0	59.0	24 h (20.0 mA cm <sup>-2</sup> )	30

**Table S3.** HER performance comparison of C@Pt/CNTs-325 ( $\eta^{1000}$ ) with those reported.

Catalyst	Electrolyte	$\eta^{1000}$ (mV)	Stability	Ref.
C@Pt/CNTs-325	0.5 M H <sub>2</sub> SO <sub>4</sub>	95.5		This work
	1.0 M PBS	1389.8	>600 h (1.0 A cm <sup>-2</sup> )	
	1.0 M KOH	399.4		
Pt NPs@CF	0.5 M H <sub>2</sub> SO <sub>4</sub>	97.0	10000 cycles	31
Pt-Ru/CNT	0.5 M H <sub>2</sub> SO <sub>4</sub>	130.0	100 h (0.5 A cm <sup>-2</sup> )	32
Pt-Pd@NPA	0.5 M H <sub>2</sub> SO <sub>4</sub>	133.0	100 h (1.0 A cm <sup>-2</sup> )	33
P-Pt <sub>3</sub> Co/NC	0.5 M H <sub>2</sub> SO <sub>4</sub>	136.0	50 h (10.0 mA cm <sup>-2</sup> )	34
Pt@N-CTs	0.5 M H <sub>2</sub> SO <sub>4</sub>	157.9	264 h (0.5 A cm <sup>-2</sup> )	35
p-Pt <sub>3</sub> V	0.5 M H <sub>2</sub> SO <sub>4</sub>	300.0	100 h (0.5 A cm <sup>-2</sup> )	36
Ni <sub>3</sub> N/Pt	1.0 M KOH	430.0	24 h (0.05 A cm <sup>-2</sup> )	37
Pt/C-NF	1.0 M KOH	444.0	\	38
Pt foil	1.0 M KOH	822.0	\	39

**Table S4.** Performance comparison of C@Pt/CNTs-325||RuIr/TiO<sub>2</sub> with other overall water electrolyzers reported

Catalyst	Electrolyte	Input voltages (V)	Stability	Ref.
C@Pt/CNTs-325  RuIr/TiO <sub>2</sub>	0.5 M H <sub>2</sub> SO <sub>4</sub>	1.85 (1.0 A cm <sup>-2</sup> )	>1000 h (1.0 A cm <sup>-2</sup> )	This work
	1.0 M PBS	2.92 (1.0 A cm <sup>-2</sup> )		
	1.0 M KOH	1.72 (1.0 A cm <sup>-2</sup> )		
R-NF-Pt  NiFe-LDH	1.0 M KOH	1.78 (1.0 A cm <sup>-2</sup> )	400 h (1.0 A cm <sup>-2</sup> )	40
Pt/Ru NWs  RuO <sub>2</sub>	1.0 M KOH	1.90 (1.0 A cm <sup>-2</sup> )	100 h (0.2 A cm <sup>-2</sup> )	41
Pt-Ru/RuO <sub>2</sub>   NiFe-LDH	1.0 M KOH	1.77 (1.0 A cm <sup>-2</sup> )	\	42
Pt/NiO <sub>x</sub> -Ov  NiFe-LDH	1.0 M KOH	1.78 (1.0 A cm <sup>-2</sup> )	400 h (1.0 A cm <sup>-2</sup> )	40
Pt-AC/Cr-N-C  NiFe-LDH	1.0 M KOH	1.90 (1.0 A cm <sup>-2</sup> )	100 h (0.5 A cm <sup>-2</sup> )	43
Pt-Ni(OH) <sub>2</sub> @NM  RuO <sub>2</sub>	1.0 M KOH	2.24 (1.0 A cm <sup>-2</sup> )	600 h (0.4 A cm <sup>-2</sup> )	44
Co <sub>n</sub> -Pt <sub>1</sub> @NPC  NiFe-LDH	1.0 M KOH	1.97 (1.0 A cm <sup>-2</sup> )	100 h (1.0 A cm <sup>-2</sup> )	45
PtRu-CO <sub>3</sub> O <sub>4</sub>   PtRu-CO <sub>3</sub> O <sub>4</sub>	0.5 M H <sub>2</sub> SO <sub>4</sub>	1.94 (1.0 A cm <sup>-2</sup> )	200 h (0.2 A cm <sup>-2</sup> )	46
Pt/TiAl-nanocone  IrO <sub>2</sub>	0.5 M H <sub>2</sub> SO <sub>4</sub>	1.88 (1.0 A cm <sup>-2</sup> )	800 h (1.0 A cm <sup>-2</sup> )	47

## References

1. B. Ravel and M. Newville, *J. Synchrotron Rad.*, 2005, **12**, 537–541.
2. C. Wei, R. R. Rao, J. Peng, B. Huang, I. E. L. Stephens, M. Risch, Z. J. Xu and Y. Shao-Horn, *Adv. Mater.*, 2019, **31**, 1806296.
3. K. R. Cooper and M. Smith, *J. Power Sources*, 2006, **160**, 1088-1095.
4. M. B. Stevens, L. J. Enman, A. S. Batchellor, M. R. Cosby, A. E. Vise, C. D. M. Trang and S. W. Boettcher, *Chem. Mater.*, 2017, **29**, 120-140.
5. K. Liu, H. Yang, Y. Jiang, Z. Liu, S. Zhang, Z. Zhang, Z. Qiao, Y. Lu, T. Cheng and O. Terasaki, *Nat. Catal.*, 2023, **14**, 2424.
6. T. Gao, X. Tang, X. Li, S. Wu, S. Yu, P. Li, D. Xiao and Z. Jin, *ACS Catal.*, 2023, **13**, 49-59.
7. G. Kresse and J. Furthmüller, *Phys. Rev. B.*, 1996, **54**, 11169.
8. J. P. Perdew, K. Burke and M. Ernzerhof, *Phys. Rev. Lett.*, 1996, **77**, 3865.
9. S. Goedecker, M. Teter and J. Hutter, *Phys. Rev. B*, 1996, **54**, 1703.
10. S. Grimme, *J. Comput. Chem.*, 2006, **27**, 1787-1799.
11. G. Henkelman, B. P. Uberuaga and H. Jónsson, *J. Chem. Phys.*, 2000, **113**, 9901-9904.
12. K. M. Naik, E. Higuchi and H. Inoue, *Nanoscale.*, 2020, **12**, 11055-11062.
13. P. Wang, X. Zhang, J. Zhang, S. Wan, S. Guo, G. Lu, J. Yao and X. Huang, *Nat. Commun.*, 2017, **8**, 14580.
14. L. Zhai, X. She, L. Zhuang, Y. Li, R. Ding, X. Guo, Y. Zhang, Y. Zhu, K. Xu and H. J. Fan, *Angew. Chem. Int. Ed.*, 2022, **134**, e202116057.
15. Z. Xing, C. Han, D. Wang, Q. Li and X. Yang, *ACS Catal.*, 2017, **7**, 7131-7135.
16. C. Zhang, P. Wang, W. Li, Z. Zhang, J. Zhu, Z. Pu, Y. Zhao and S. Mu, *J. Mater. Chem. A*, 2020, **8**, 19348-19356.
17. J. Zhu, Y. Tu, L. Cai, H. Ma, Y. Chai, L. Zhang and W. Zhang, *Small*, 2022, **18**, 2104824.
18. Z. Wang, B. Xiao, Z. Lin, Y. Xu, Y. Lin, F. Meng, Q. Zhang, L. Gu, B. Fang and S. Guo, *Angew. Chem. Int. Ed.*, 2021, **60**, 23388-23393.
19. S. Jiao, M. Kong, Z. Hu, S. Zhou, X. Xu and L. Liu, *Small*, 2022, **18**, 2105129.
20. Q. Dang, Y. Sun, X. Wang, W. Zhu, Y. Chen, F. Liao, H. Huang and M. Shao, *Appl. Catal. B-Environ.*, 2019, **257**, 117905.
21. H. Jin, Z. Xu, Z.-Y. Hu, Z. Yin, Z. Wang, Z. Deng, P. Wei, S. Feng, S. Dong, J. Liu, S. Luo, Z. Qiu, L. Zhou, L. Mai, B.-L. Su, D. Zhao and Y. Liu, *Nat. Commun.*, 2023, **14**, 1518.
22. Z. Zhao, H. Liu, W. Gao, W. Xue, Z. Liu, J. Huang, X. Pan and Y. Huang, *J. Am. Chem.*

- Soc.*, 2018, **140**, 9046-9050.
23. H. J. Song, M.-C. Sung, H. Yoon, B. Ju and D.-W. Kim, *Adv. Sci.*, 2019, **6**, 1802135.
  24. J. Cai, X. Liao, P. Li, Q. Wang, H. Huang, Z. Lyu, J. Lin and S. Xie, *Chem. Eng. J.*, 2022, **429**, 132414.
  25. Y. Tan, R. Xie, S. Zhao, X. Lu, L. Liu, F. Zhao, C. Li, H. Jiang, G. Chai and D. J. Brett, *Adv. Funct. Mater.*, 2021, **31**, 2105579.
  26. H. Zhang, P. An, W. Zhou, B. Guan, P. Zhang, J. Dong and X. Lou, *Sci. Adv.*, 2018, **4**, eaao6657.
  27. J. Chen, Y. Yang, J. Su, P. Jiang, G. Xia and Q. Chen, *ACS Appl. Mater. Interfaces*, 2017, **9**, 3596-3601.
  28. J. Zhang, E. Wang, S. Cui, S. Yang, X. Zou and Y. Gong, *Nano Lett.*, 2022, **22**, 1398-1405.
  29. X. Li, J. Yu, J. Jia, A. Wang, L. Zhao, T. Xiong, H. Liu and W. Zhou, *Nano Energy*, 2019, **62**, 127-135.
  30. Y. Yan, R. Zhang, Y. Yu, Z. Sun, R. Che, B. Wei, A. P. LaGrow, Z. Wang and W. Zhou, *Appl. Catal. B-Environ.*, 2021, **291**, 120100.
  31. Q. Li, Z. Deng, D. Tao, J. Pan, W. Xu, Z. Zhang, H. Zhong, Y. Gao, Q. Shang and Y. Ni, *Adv. Funct. Mater.*, 2024, **34**, 2411283.
  32. D. Zhang, Z. Wang, X. Wu, Y. Shi, N. Nie, H. Zhao, H. Miao, X. Chen, S. Li and J. Lai, *Small*, 2022, **18**, 2104559.
  33. C. Yang, H. Lei, W. Zhou, J. Zeng, Q. Zhang, Y. Hua and C. Xu, *J. Mater. Chem. A*, 2018, **6**, 14281-14290.
  34. C. Li, C. Tian, H. Tang, M. Liu, L. Zheng, F. Huang, G.-R. Li and Q. Li, *ACS Energy Lett.*, 2023, **8**, 5161-5169.
  35. Q. Pan, Y. Wang, B. Chen, X. Zhang, D. Lin, S. Yan, F. Han, H. Zhao and G. Meng, *Small*, 2024, **20**, 2309067.
  36. Y. Da, R. Jiang, Z. Tian, G. Chen, Y. Xiao, J. Zhang, S. Xi, Y. Deng, W. Chen and X. Han, *Adv. Energy Mater.*, 2023, **13**, 2300127.
  37. Y. Wang, L. Chen, X. Yu, Y. Wang and G. Zheng, *Adv. Energy Mater.*, 2017, **7**, 1601390.
  38. S. Xue, Z. Liu, C. Ma, H.-M. Cheng and W. Ren, *Sci. Bull.*, 2020, **65**, 123-130.
  39. Y. Luo, L. Tang, U. Khan, Q. Yu, H.-M. Cheng, X. Zou and B. Liu, *Nat. Commun.*, 2019, **10**, 269.
  40. K. Wang, S. Wang, K. S. Hui, J. Li, C. Zha, D. A. Dinh, Z. Shao, B. Yan, Z. Tang and K. N. Hui, *Adv. Funct. Mater.*, 2023, **33**, 2211273.
  41. J. Yan, R. Wu, G. Jin, L. Jia, G. Feng and X. Tong, *Adv. Powder Mater.*, 2024, **3**, 100214.

42. Y. Zhu, M. Klingenhof, C. Gao, T. Koketsu, G. Weiser, Y. Pi, S. Liu, L. Sui, J. Hou, J. Li, H. Jiang, L. Xu, W.-H. Huang, C.-W. Pao, M. Yang, Z. Hu, P. Strasser and J. Ma, *Nat. Commun.*, 2024, **15**, 1447.
43. L. Zeng, Z. Zhao, Q. Huang, C. Zhou, W. Chen, K. Wang, M. Li, F. Lin, H. Luo, Y. Gu, L. Li, S. Zhang, F. Lv, G. Lu, M. Luo and S. Guo, *J. Am. Chem. Soc.*, 2023, **145**, 21432-21441.
44. J. Zhang, J. Dang, X. Zhu, J. Ma, M. Ouyang and F. Yang, *Appl. Catal. B-Environ.*, 2023, **325**, 122296.
45. Y. Xu, J. Du, J. Jiang, Y. Miao, Z. Zhuang, Z. Liu, Y. Yan, R. Pan, J. Yang and M. Wang, *Angew. Chem. Int. Ed.*, 2025, e202502227.
46. D. Li, D. Xu, Y. Pei, Q. Zhang, Y. Lu and B. Zhang, *J. Am. Chem. Soc.*, 2024, **146**, 28728-28738.
47. T. Chen, J. Ma, C. Liang, Y. Luo, X. Xu, J. Hu, J. Chen and W. Ding, *Adv. Mater.*, 2025, 2418527.